International Journal of Heat and Mass Transfer 105 (2017) 81–89

Contents lists available at ScienceDirect

International Journal of Heat and Mass Transfer

journal homepage: www.elsevier.com/locate/ijhmt

The optimization of channels for a proton exchange membrane fuel cell applying genetic algorithm

Xiangbing Zeng [a], Ya Ge [a], Jun Shen [a], Lingping Zeng [b], Zhichun Liu [a,*], Wei Liu [a,*]

[a] School of Energy and Power Engineering, Huazhong University of Science and Technology, 430074 Wuhan, China
[b] Department of Mechanical Engineering, Massachusetts Institute of Technology, Cambridge, MA 02139-4307, United States

ARTICLE INFO

Article history:
Received 22 July 2016
Received in revised form 14 September 2016
Accepted 22 September 2016
Available online 26 September 2016

Keywords:
Channel optimization
Proton exchange membrane fuel cell
Genetic algorithm
Mass transport

ABSTRACT

A channel is a significant part of a proton exchange membrane fuel cell (PEMFC), and the configuration of the channel has a great effect on the mass transfer of the PEMFC, which directly influences the performance. In this study, a three-dimensional, single-phase, and non-isothermal model of a PEMFC with a single straight channel is developed. Based on the model, genetic algorithm (GA) is adopted to obtain an optimal design of the channel configuration. Power consumption of flow and output power of a PEMFC are considered into the objective function, and the width of bottom and top edges of the channel, in both the anode and cathode sides, are selected as variables. The optimal design obtained is a trapezoidal channel. At an operating potential of 0.4 V, the increment in current density in the optimal design is 10.92% compared to a basic design having a square channel. Moreover, the optimal design shows more uniform distributions of reactants and current density than the basic design.

1. Introduction

Proton exchange membrane fuel cell (PEMFC) technology is a type of green energy technology because it utilizes hydrogen, which is a renewable energy resource, as fuel. In a PEMFC, the chemical energy of reactants is converted directly into electricity [1], and the byproducts are water and heat. Therefore, a PEMFC is considered an ideal alternative to future power sources [2]. In addition, because of the advantages of high power density, low emissions, and fast startup, a PEMFC has wide application prospects in the automotive field and portable electronic devices. However, high manufacturing cost and low reliability make it difficult for widespread commercial use. Therefore, the performance of a PEMFC needs to be improved further.

Diffusion of hydrogen and oxygen through the gas diffusion layer (GDL) and the distributions of these species in the catalyst layer are important determinants of PEMFC performance [3]. The channel of a PEMFC plays an important role in the transportation and distribution of reactants. Therefore, changing the geometrical configuration of the channel to obtain an optimal channel configuration is an important aspect of improving PEMFC performance. During the past decades, many researchers have made great efforts to improve the PEMFC performance by optimizing the configuration of the channel.

Ahmed et al. [3] studied the influence of rectangular, trapezoidal, and parallelogram cross-sections of a channel on the performance of a PEMFC, and they observed higher cell voltage in the rectangular channel, but more uniform reactant and current density distributions in the trapezoidal channel. Manso et al. [4] developed three-dimensional models with different channel height/width ratio to investigate the influence of the channel cross-section aspect ratio on the performance of a PEMFC. Yoon et al. [5] adopted an experimental method to investigate the effects of channel and rib width on the performance of a PEMFC. Their results indicated that a narrow rib width could improve the performance of a PEMFC. Bilgili et al. [6] added obstacles near the outlet of a channel and compared the difference in performance between the channel with obstacles and a straight channel. In their study, they observed that the obstacles could improve the reactants distribution along the channels and facilitate the transport of reactants through the GDL, which could enhance the PEMFC performance. Shimpalee et al. [7] used a three-dimension model with a serpentine channel to study the effects of channel and rib width on PEMFC performance. They observed that a narrower channel with a wider rib spacing showed a higher performance. Liu et al. [8] conducted studies on a two-dimensional model of a PEMFC with a tapered flow field design. It was observed that the tapered flow channel could force more reactants into the GDL

* Corresponding authors.
E-mail addresses: zcliu@hust.edu.cn (Z. Liu), w_liu@hust.edu.cn (W. Liu).

http://dx.doi.org/10.1016/j.ijheatmasstransfer.2016.09.068
0017-9310/

Nomenclature

A	effective catalyst area per unit volume ($m^2\ m^{-3}$)
C	molar concentration ($mol\ m^{-3}$)
D	mass diffusivity of species ($m^2\ s^{-1}$)
F	Faraday's number 96,487 ($C\ mol^{-1}$)
j	transfer current density ($A\ m^{-3}$)
R	universal gas constant 8.314 ($J\ mol^{-1}\ K^{-1}$)
S	source term
T	temperature (K)
$\mathbf{u}$	velocity ($m\ s^{-1}$)
k	thermal conductivity (W/m K)
K	permeability (m^2)
M	molecular weight
p	pressure (Pa)
C_p	constant-pressure heat capacity ($J\ kg^{-1}\ K^{-1}$)

Greek letters

α	transfer coefficient or water transport coefficient
ε	porosity
μ	viscosity ($Pa\ s^{-1}$)
ρ	density ($kg\ m^{-3}$)
σ	conductivity ($S\ m^{-1}$)
ϕ	phase potential
ω	species mass fraction
η	overpotential (V)

Subscripts

a	anode
c	cathode
eff	effective
ref	reference
k	H_2 or O_2
e	electrolyte
s	electron
aggl	agglomerate

and catalyst layer, which in turn increased the output power. Tiss et al. [9] added partial blocks in a channel and analyzed three different designs whose the tilt angles of partial blocks were 4.9°, 6.6° and 8.2°, respectively. Their results indicated that the performance of a PEMFC was best when the tilt angle was 4.9°. Liu et al. [10] applied a baffle-blocked flow channel in the cathode of a two-dimensional fuel cell model. They observed that the reactant transport and the performance of the PEMFC were enhanced by the baffles. Kuo et al. [11] developed a three-dimensional, single-phase, multi-species, steady-state model of a PEMFC with wave-like flow channels and compared its performance with that of a conventional straight channel at temperatures of 323 K, 333 K and 343 K. The results indicated that the PEMFC with wave-like channels obtained a higher power density. Hu et al. [12,13] compared the interdigitated flow field with the conventional flow field. They found the interdigitated flow filed made the fuel cell had better mass transfer performance. Wang et al. [14] changed the flow channel size to find the effect of the flow channel size on the cell performance for single serpentine flow field designs. The results shown that decreases of the flow channel and rib size led to more uniform current density distributions and more pressure drop. Wang et al. [15] proposed a novel serpentine-baffle flow field design for enhancing the performance of fuel cell. Roshandel et al. [16] established three fuel cell models with parallel flow channels, serpentine flow channels and bio inspired flow channel respectively. The bio inspired flow channel shown higher performance. Some other researchers [17–20] also proposed new channel designs for improving the performance of fuel cell.

In the studies mentioned above, a PEMFC was optimized using several specific configurations of the channel. However, few researchers adopted optimization algorithms to optimize the configuration of a PEMFC.

Perng et al. [21] investigated the effect of a tapered flow channel with a baffle plate on the performance of a PEMFC by developing a two-dimensional non-isothermal cathode model and used the element-by-element preconditioned conjugate gradient method to optimize the tapered ratio and gap ratio. Wang et al. [22] optimized the height and width of a serpentine channel PEMFC by adopting a simplified conjugate-gradient method. Yang et al. [23] conducted studies on a two-dimensional PEMFC model to optimize its configuration by using genetic algorithm. The widths of channel and rib and the channel height were chosen as geometric variables. They observed that the performance of a wider channel was better than a narrower channel, and a channel height of 0.515 mm showed the best performance. However, in their study, the evaluation criteria of PEMFC performance did not include pressure drop due to the flow of reactants in the PEMFC that could lead to extra power consumption.

In this study, a three-dimensional PEMFC model with a straight single channel is developed, and the results are verified with experimental data. Based on the model, genetic algorithm is used to obtain the best cross-section of the channel, and both output power and pressure drop are considered in the objective function.

2. Model development

The model developed in this study is a three-dimensional, steady-state, single-phase, and non-isothermal PEMFC model.

2.1. Model assumptions

To make the model manageable, the present model is developed under the following assumptions:

1. The flow in the fuel cell is laminar.
2. The gas mixtures are considered ideal, and ideal gas law was employed for gas mixtures.
3. Water in the fuel cell is assumed to be in the gaseous phase.
4. The membrane is assumed to be fully humidified because of 100% humidity in the anode and cathode, and its protonic conductivity is simplified to be a constant [24].

2.2. Governing equations

As shown in Fig. 1, the fuel cell geometry used in this model consists of nine components (anode and cathode bipolar plates, flow channels, GDLs, catalyst layers, and membrane). The geometric parameters of the model, which correspond to the experiment test case of [25], are listed in Table 1. Each component has different governing equations. In this study, the governing equations mainly involve the continuity, momentum, energy, electrochemical, and Maxwell–Stafen equations. The corresponding governing equations are written as follows:

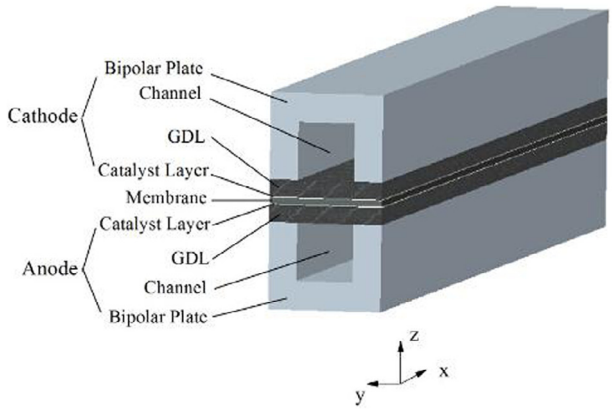

Fig. 1. Fuel cell geometry.

Table 1
Geometric parameters.

Parameters	Value [m]
Cell width	2.0×10^{-3}
Channel length	0.02
Channel height	1.0×10^{-3}
Channel width	1.0×10^{-3}
Rib width	1.0×10^{-3}
GDL thickness	0.3×10^{-3}
Catalyst layer thickness	1.29×10^{-5}
Membrane thickness	0.108×10^{-3}

Continuity equation

$$\nabla \cdot (\rho \mathbf{u}) = S_{\mathrm{m}} \tag{1}$$

where S_{m} is the mass source term, which is only available for anode and cathode catalyst layers. For the anode catalyst layer: $S_{\mathrm{m}} = -\frac{j_{\mathrm{a,eff}}}{2F} M_{\mathrm{H_2}} - \frac{\alpha j_{\mathrm{a,eff}}}{F} M_{\mathrm{H_2}}$. For the cathode catalyst layer: $S_{\mathrm{m}} = -\frac{j_{\mathrm{c,eff}}}{4F} M_{\mathrm{O_2}} + \frac{(1+2\alpha)}{2F} j_{\mathrm{c,eff}} M_{\mathrm{O_2}}$.

Momentum equation

$$\frac{1}{\varepsilon^2} \nabla \cdot (\rho \mathbf{u}\mathbf{u}) = -\nabla p + \frac{1}{\varepsilon} \nabla \cdot (\mu \nabla \mathbf{u}) + S_{\mathrm{mom}} \tag{2}$$

where S_{mom} is the momentum source term. For the GDL and catalyst layer, $S_{\mathrm{mom}} = -\frac{\mu}{K}\mathbf{u}$.

Energy equation

$$\rho C_{\mathrm{p}} \mathbf{u} \cdot \nabla T = \nabla \cdot (k_{\mathrm{eff}} \nabla T) + S_{\mathrm{T}} \tag{3}$$

where k_{eff} is the effective thermal conductivity. For the GDL and catalyst layer, the effective thermal conductivity can be expressed as [24]:

$$k_{\mathrm{eff}} = \varepsilon k_{\mathrm{f}} + (1-\varepsilon) k_{\mathrm{s}} \tag{4}$$

where k_{f} is the thermal conductivity of fluid, and k_{s} is the thermal conductivity of solid.

In the channel, GDL, and catalyst layer, the multi-component diffusion and convection are solved by Maxwell–Stafen equation. The general form of the Maxwell–Stafen equation is shown below:

$$\nabla \cdot \left[-\rho \omega_i \sum_{j=1}^{N} D_{ij,\mathrm{eff}} \left\{ \frac{M}{M_j} \left(\nabla \omega_j + \omega_j \frac{\nabla M}{M} \right) + (x_j - \omega_j) \frac{\nabla p}{p} \right\} \right] + \rho \mathbf{u} \cdot \nabla \omega_i = S_i \tag{5}$$

where $D_{ij,\mathrm{eff}}$ is the effective species diffusivity, and S_i is the species source term.

The effect of porous media (GDL and catalyst layer), which is described by Bruggeman's equation, is considered in the effective species diffusivity $D_{ij,\mathrm{eff}}$. The Bruggeman's equation is given below [26]:

$$D_{ij,\mathrm{eff}} = \varepsilon^{1.5} D_{ij} \tag{6}$$

where D_{ij} is the binary diffusivity. Different literatures have predicted different theoretical binary diffusivity values, and in this study, the binary diffusivity value predicted by [26] is considered:

$$D_{ij} = D_{ij,\mathrm{ref}} \left(\frac{T}{T_{\mathrm{ref}}} \right)^{1.75} \tag{7}$$

In Eq. (5), S_i is the species source term, which is used to describe the consumption of reaction gas and the generation of water in the anode and cathode catalyst layers [27].

$$S_{\mathrm{H_2}} = -\frac{j_{\mathrm{a,eff}}}{2F} M_{\mathrm{H_2}} \tag{8}$$

$$S_{\mathrm{O_2}} = -\frac{j_{\mathrm{c,eff}}}{4F} M_{\mathrm{O_2}} \tag{9}$$

$$S_{\mathrm{H_2O}} = \frac{j_{\mathrm{c,eff}}}{2F} M_{\mathrm{H_2O}} \tag{10}$$

For the calculation of the effective electrochemical reaction rates $j_{\mathrm{a,eff}}$ and $j_{\mathrm{c,eff}}$ in the catalyst layer, a simplified agglomerate model is adopted to describe the variables. The specific expression of the simplified agglomerate model is shown as follows:

$$j_{i,\mathrm{eff}} = \eta_{aggl} j_i \tag{11}$$

where η_{aggl} is the effectiveness factor, which is used to modify the electrochemical reaction rate j_i in consideration of the effect of diffusion resistance through the catalyst with porous and agglomerate structure. According to [27], the effectiveness factor η_{aggl} is expressed as follows:

$$\eta_{aggl} = \frac{3}{\phi_L} \left(\frac{1}{\tanh(\phi_L)} - \frac{1}{\phi_L} \right), \quad \phi_L = L_{aggl} \sqrt{\frac{|j_i|}{C_i D_i^{\mathrm{m}}}} \tag{12}$$

where ϕ_L is the Thiele modulus, L_{aggl} is the characteristic length of the catalyst particle, j_i is the electrochemical reaction rate, and D_i^{m} is the species diffusivity in the polymer phase.

The Bulter–Volmer equation is used to describe the electrochemical reaction rate j_i, which can be expressed as follows:

$$j_i = A j_{i,\mathrm{ref}} \left(\frac{C_k}{C_{k,\mathrm{ref}}} \right)^{\gamma_i} \left(e^{\frac{\alpha_a F}{RT}\eta_a} - e^{\frac{\alpha_c F}{RT}\eta_c} \right) \tag{13}$$

where $j_{i,\mathrm{ref}}$ is the reference exchange current density, and η_{a} and η_{c} are the activation overpotential. i could be a and c standing for anode and cathode, respectively.

The cathodic value of the reference exchange current density $j_{i,\mathrm{ref}}$ is several orders of magnitude smaller than the anodic value because of the tardiness of oxygen reduction reaction at the cathode. Therefore, the cathode exhibits significant activation overpotential during cell operation [28]. The relation of cathode reference exchange current density is shown as follows:

$$j_{\mathrm{c,ref}} = 10^4 \exp\left(3.507 - \frac{4001}{T} \right) \tag{14}$$

The overpotential in the anode side is $\eta_a = \phi_{\mathrm{s}} - \phi_{\mathrm{e}}$, and in the cathode side, $\eta_c = \phi_{\mathrm{s}} - \phi_{\mathrm{e}} - U_0$. U_0 is the open-circuit potential, which is the theoretical voltage that can be delivered by the PEMFC. According to [29], the expression of open-circuit potential is

$$U_0 = 1.23 - 0.9 \times 10^{-3} (T - 298) \tag{15}$$

Furthermore, the charge conservation equation is applied for determining the solid phase potential ϕ_s and the electrolyte phase potential ϕ_e.

Proton conservation equation:

$$\nabla \cdot (\sigma_e \nabla \phi_e) + S_e = 0 \tag{16}$$

Electron conservation equation:

$$\nabla \cdot (\sigma_s \nabla \phi_s) + S_s = 0 \tag{17}$$

The operation and electrochemical parameters for the straight channel fuel cell section are summarized in Table 2.

2.3. Boundary conditions

For reducing computational cost, we apply symmetry boundary conditions in the y direction. The no-flux conditions are applied in the x direction except for the inlets and outlets. At the anode and cathode inlets, the velocity, temperature and species mass fraction are specified. The inlet species mass fraction, $\omega_{k,in}$, can be calculated by the inlet pressure and relative humidity of inlet gases. The cathode and anode inlet velocities are prescribed by:

$$u_{in,c} = \zeta_c \frac{i_{max}}{4F} A_m \frac{1}{\omega_{O_2,in}} \frac{RT_{in,c}}{p_{in,c}} \frac{1}{A_{ch}} \tag{18}$$

and

$$u_{in,a} = \zeta_a \frac{i_{max}}{2F} A_m \frac{1}{\omega_{H_2,in}} \frac{RT_{in,a}}{p_{in,a}} \frac{1}{A_{ch}} \tag{19}$$

where i_{max} is the maximum average current density, A_m is the geometrical area of the membrane and A_{ch} is the channel cross-section area.

At the outlets, only the pressure is set to be the operating pressure. The gradient for other variables in the x direction is specified as zero.

At the x–y planes boundaries, i.e. the surfaces of the bipolar plates, the potential is prescribed. At the anode side, the potential is set to be zero. At the cathode side, the value of potential varies from 0.9 V to 0.4 V with a step of 0.05 V.

Table 2
Operation and electrochemical parameters.

Description	Value	Reference
Operating temperature (T)	343.14 K	[25]
Inlet temperature, anode and cathode (T_{in})	343.14 K	[25]
Anode stoichiometric flow rate (ζ_a)	3	[25]
Cathode stoichiometric flow rate (ζ_c)	3	[25]
Relative humidity of inlet gases	100%	[25]
Operating pressure (p)	1 atm	[25]
GDL porosity (ε)	0.4	[25]
Permeability (K)	1.76×10^{-11} m^2	[25]
Anode volumetric exchange current density ($Aj_{a,ref}$)	1.05e10 A/m^3	Assumed
Cathode volumetric exchange current density ($Aj_{c,ref}$)	100 A/m^3	Assumed
Oxygen reference concentration ($C_{O_2,ref}$)	56.4 mol/m^3	[30]
Hydrogen reference concentration ($C_{H_2,ref}$)	3.39 mol/m^3	[30]
Reference binary diffusivity of H_2 in H_2O ($D_{H_2-H_2O,ref}$)	0.915 cm^2/s	[1]
Reference binary diffusivity of O_2 in H_2O ($D_{O_2-H_2O,ref}$)	0.282 cm^2/s	[1]
Reference binary diffusivity of O_2 in N_2 ($D_{O_2-N_2,ref}$)	0.220 cm^2/s	[1]
Reference binary diffusivity of H_2O in N_2 ($D_{H_2O-N_2,ref}$)	0.256 cm^2/s	[1]

2.4. Solution technique

The governing equations and boundary conditions described above are solved by finite element method in a commercial software COMSOL Multiphysics 5.0 and a parametric segregated solver is chosen to be the solver. In order to check the mesh independency, three different grids are employed. The elements of these three girds are 35910, 54900 and 85400, respectively and all elements are hexahedron. The current density of PEMFC is computed under three different grids when the operating potential is 0.5V. As shown in Fig. 2, the differences in current density between the grids with 54900 and 85400 elements are less than 0.05%. In this paper, the grid with 54900 elements is used for the simulation of PEMFC. The simulation of PEMFC for each operating potential requires about 10 min on an Intel Xeon 2.4 GHz workstation with a 32.0 GB RAM.

2.5. Model validation

To validate the results obtained by the model, the fuel cell polarization curve of the simulation is compared with the experimental data of Wang et al. [25] that is shown in Fig. 2.

As can be seen in Fig. 3, the result of simulation shows good agreement with the experiment data. There just exists a small difference between the simulation data and experiment data. Therefore, in this paper, this model is used to be the basic model for the optimization of the channel structure.

3. Genetic algorithm optimization

Genetic algorithm is a method of obtaining the optimal solution by simulating a natural evolution process (the genetic mechanism of the survival of the fittest). It has inherent implicit parallelism and better global optimization ability. Therefore, in this paper, genetic algorithm is chosen to be the optimization method to optimize the configuration of the channel. The commercial mathematics software MATLAB is used as the tool that connects the genetic algorithm with COMSOL Multiphysics. The combination of numerical simulation and optimization algorithm is an efficient method to find the optimal structure. This kind of method can be found in [23,31,32].

In this study, based on the above model, three geometric parameters of the channel, the width of the bottom edge, the width of the top edge, and the height denoted by a, b, and c, respectively, are considered, as shown in Fig. 4. To keep the reactant flow rate

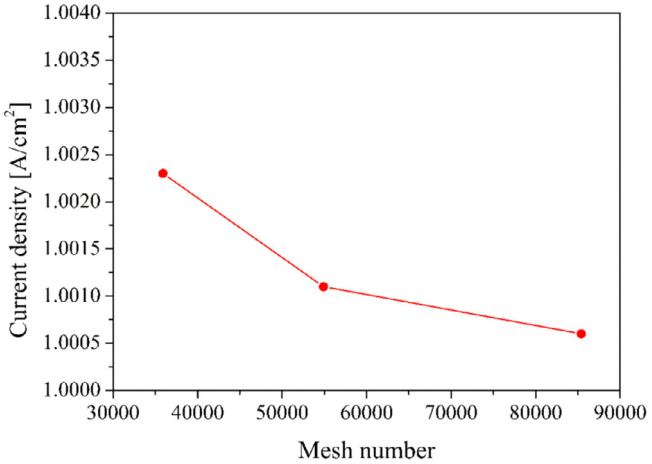

Fig. 2. Grid independent test.

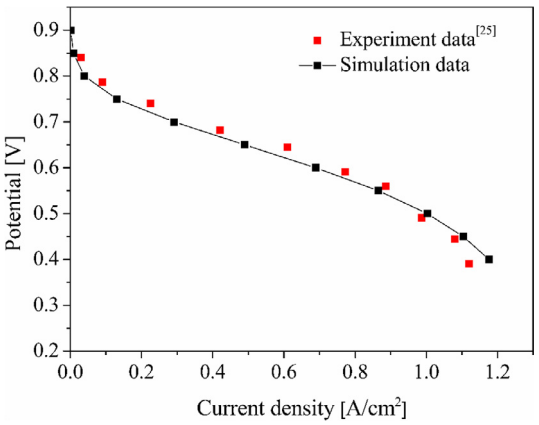

Fig. 3. Polarization curve: comparison of simulation and experiment.

and the inlet boundary condition the same during the optimization process, the cross-sectional area is kept constant, i.e., $a + b \cdot c/2 = 1\ \text{mm}^2$. We select the width of the bottom edge a and the width of the top edge b as variables, and the height c is a dependent variable. Other parameters, such as the width and length of the fuel cell, are constant. The purpose of that is to obtain an optimal channel configuration that can yield the best performance for a fuel cell for the same volume of the fuel cell. The ranges of variables a and b are specified as follows:

$$1.0\ \text{mm} < a < 1.7\ \text{mm} \qquad 0.6\ \text{mm} < b < 1.7\ \text{mm}$$

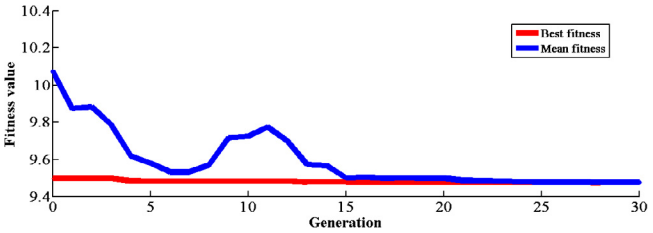

Fig. 6. Optimization results.

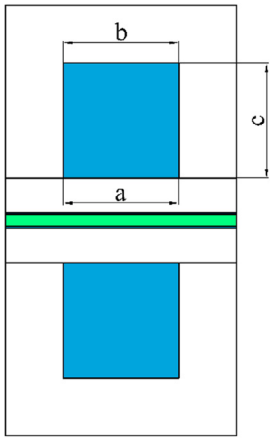

Fig. 4. Cross-sectional view of the PEMFC model.

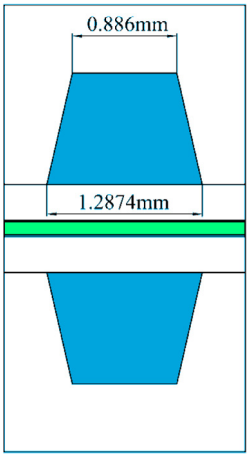

Fig. 7. The cross-sectional view of optimal design.

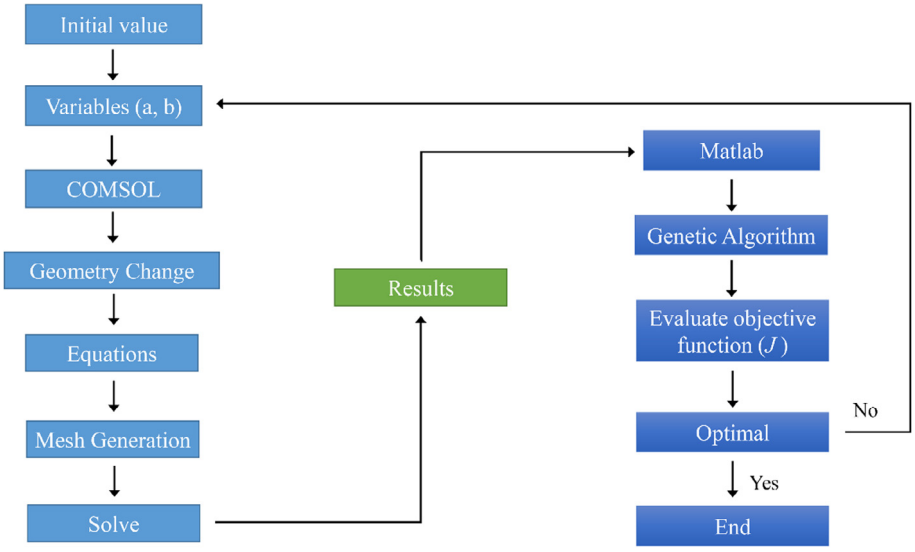

Fig. 5. Flow chart of the optimization process.

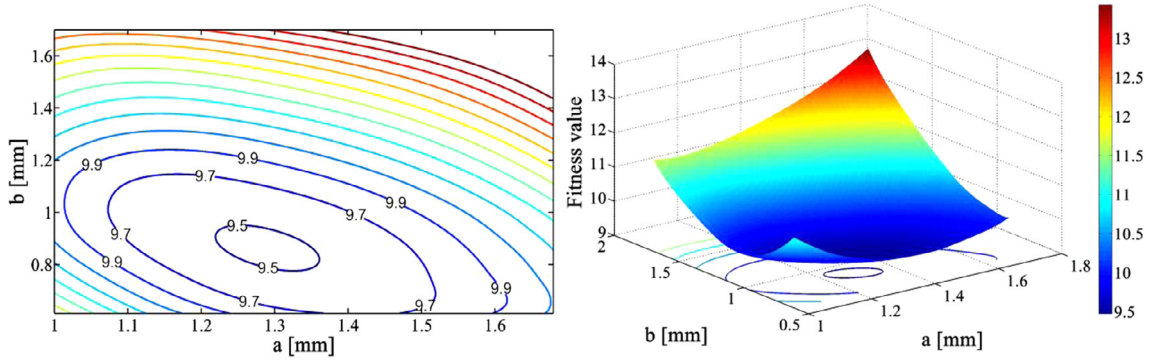

Fig. 8. Contour map of the fitness value.

Table 3
Comparison between the optimal design and the basic design.

Parameters	Basic design	Optimal design
Fitness value	9.92	9.47
Pressure drop (pa)	4.713	4.866
Current density (A/cm^2)	1.001	1.082

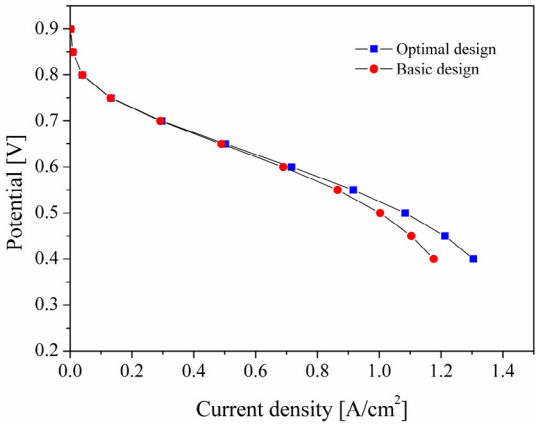

Fig. 9. Comparison between polarization curves for the optimal design with basic design.

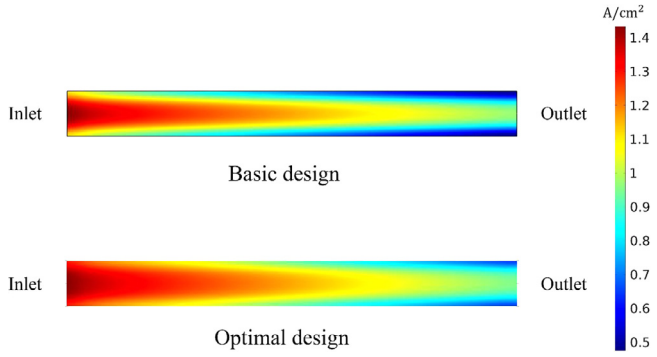

Fig. 10. Current density distribution in the membrane at 0.5 V.

Furthermore, the objective function is chosen as,

$$J = k\frac{\Delta p_c \cdot u_{\mathrm{in,c}} \cdot A_{\mathrm{ch}}}{V_{\mathrm{cell}} \cdot i_{\mathrm{ave}} \cdot A_{\mathrm{m}}} \tag{20}$$

The numerator of objective function which is the power consumption of flow of fuel cell is the product of cathode pressure drop Δp_c, inlet velocity $u_{\mathrm{in,c}}$ and the cross-sectional area of channel

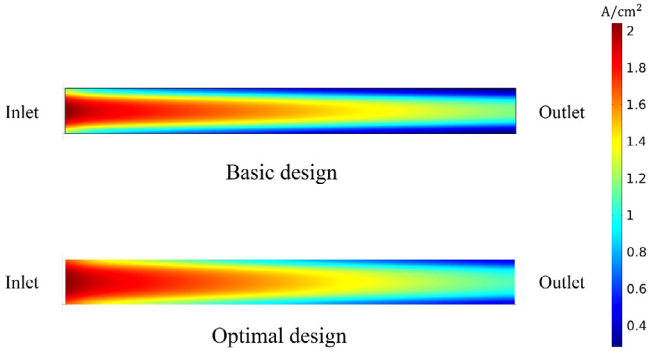

Fig. 11. Current density distribution in the membrane at 0.4 V.

A_{ch}. Because the cathode reactant is provided by the compressor and the anode reactant is provided by the pressure tank, only the cathode power consumption is considered in this study. In addition, the denominator, which represents the output power of the fuel cell, is the product of the fuel cell operational potential V_{cell}, average current density i_{ave}, and activated area A_{m}. k is a constant whose value is 1e6. When the value of objective function reaches the minimum, the performance of the fuel cell is best.

When the optimization start, the variables a and b are automatically generated from the genetic algorithm. Each pair of a and b are considered as an individual of the population, which carry the genes. The values of a and b then enter into Comsol Multiphysics to calculate the fitness value derived from the objective function, whose value decides the performance of the PEMFC. Finally, the fitness value return to the genetic algorithm for evaluation. The individual who has a better performance will be considered as genetic for the next generation. In this genetic process, three genetic operators, selection, crossover, and mutation, are involved. The best individual can be obtained by performing the optimization process repeatedly. The flow chart of the optimization process is shown in Fig. 5.

During the optimization process, the operational voltage is a constant. In this study, 0.5 V is chosen as the constant operational potential, referring to [23]. Because of the heavy computational burden of the genetic algorithm and the fact that only two variables are considered, the population size and generation number for the terminal condition are selected as 20 and 30, respectively.

4. Results and discussion

4.1. Optimization results

After the optimization finish, as shown in Fig. 6, the mean fitness value is identical with the best fitness value that means all

the individuals in the population achieve the best. The minimum fitness value obtained is 9.47, and the corresponding values of *a* and *b* are 1.2874 mm and 0.886 mm, respectively, as shown in Fig. 7. The best cross-sectional shape of the channel is a trapezoid, whose bottom edge is wider and top edge is narrower compared with the basic channel. In the optimal design, the contact area between flow channel and diffusion layer is larger. It can be beneficial for the mass transfer of the PEMFC that will be discussed in the next section.

In order to further analyze the optimization results, all the results computed in the optimization process are drawn in the contour map of the fitness value as shown in Fig. 8. It can be observed that a ranges from 1.22 to 1.37 mm and b ranges from 0.8 to 0.9 mm. The fitness value in this range is less than 9.5, which means that the PEMFC performance is better.

4.2. Discussion

In this section, a comparison between the optimal design and the basic design is conducted. The PEMFC performance and distributions of current density and reactants for the optimal and basic designs are analyzed.

In Table 3, the values of some parameters of the basic and optimal designs are listed for comparison. Because of the short channels of the computational domain in this study and a low Reynolds number flow in the PEMFC, the pressure drop of both the basic and optimal designs is small. The pressure drop of the optimal design is 3.25% higher than that of the basic design. However, the current density of the optimal design increases by 8.09% compared to the basic design. The optimal design is more costly, but it has greater benefits than the basic design.

Fig. 9 shows the comparison between polarization curves for the optimal and basic designs. The results show that after the optimization process, the overall performance of the PEMFC improves greatly. When the operating potential is greater than 0.7 V, the discrepancy between the polarization curves is negligible. However, the discrepancy increases with decreasing potential when the operating potential is below 0.7 V. At a potential of 0.4 V, the increment in current density with respect to the basic design is 10.92%.

Figs. 10 and 11 show the current density distribution in the membrane when the operating potential is 0.5 V and 0.4 V, respectively. It is observed that the current density under the channel is higher than that under the rib. Moreover, because of the same inlet boundary condition, the maximum current density values of these two designs are the same. The maximum current density occurs at the inlet of the channel where the concentration of the reactants is maximum. As can be seen from the difference between Figs. 10 and 11, the current density distribution at 0.4 V is relatively uneven. When the PEMFC operates at a low potential, the electrochemical reaction rate is faster, and the reactants are consumed faster, which leads to lower concentration of reactants at the region near the outlet and under the rib, as can be seen in Figs. 12 and 13. The low concentration of reactants can lead to uneven current density distribution. Compared with the basic design, at both 0.5 V and 0.4 V, the current density distribution of the optimal design is more uniform. The uniform current density distribution can give rise to a uniform temperature distribution for the PEMFC system that will cause less mechanical tension and lead to a longer service life.

In Figs. 12 and 13, contour planes are used to describe the molar concentration of the reactants in the anode and cathode sides for both the basic and optimal designs, respectively. The distributions of the reactants are similar to that of the current density. When the operating potential is lower, the distribution of reactants is more uneven.

Comparing the distributions of hydrogen and oxygen, it can be seen that the hydrogen concentration is more uniform compared

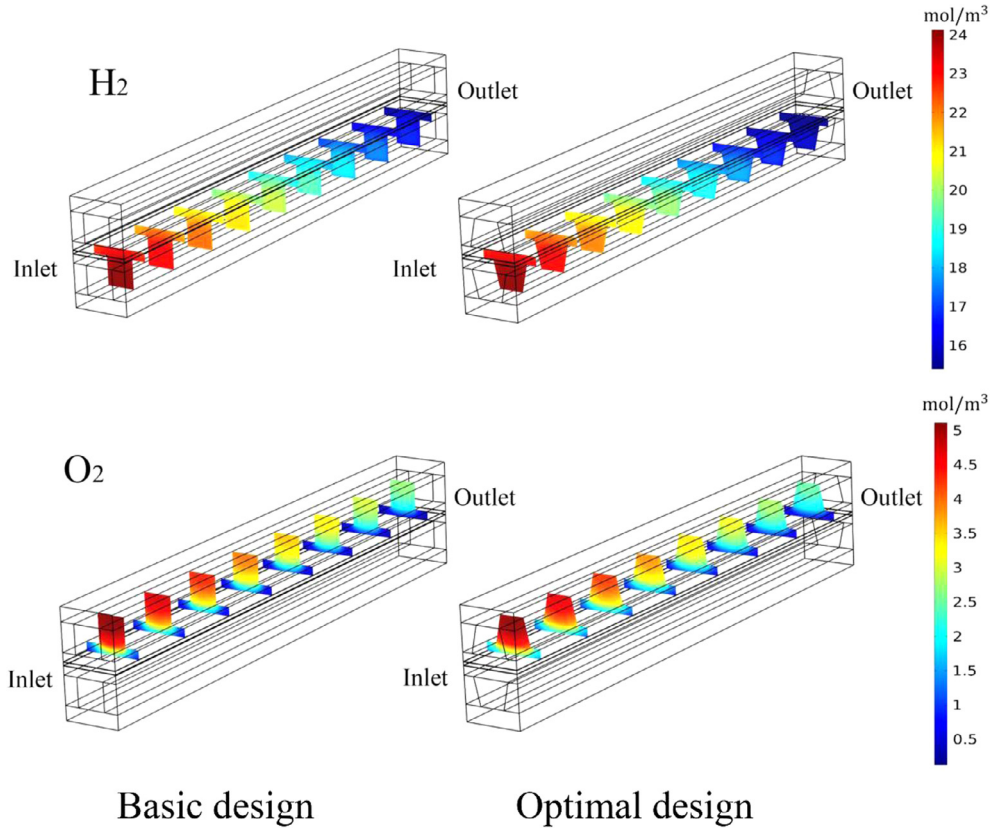

Fig. 12. Molar concentration of reactants at 0.5 V.

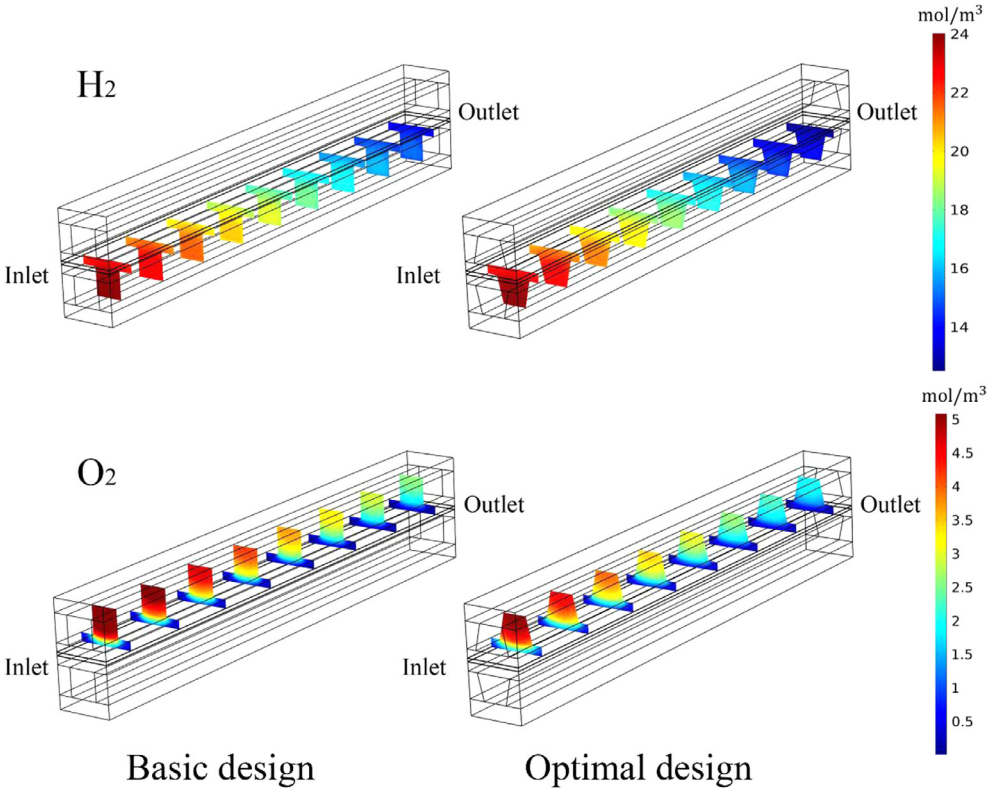

Fig. 13. Molar concentration of reactants at 0.4 V.

to the oxygen concentration at each plane for both the basic and optimal designs. The reason why the change of hydrogen concentration is small in the channel, GDL, and catalyst layer is that hydrogen has a higher diffusivity than oxygen. In the optimal design, the concentration of hydrogen is smaller at the outlet region compared to the basic design. It indicates that the optimal channel enables the electrochemical reaction in the PEMFC to proceed at a faster rate because of the faster consumption of hydrogen. The electrochemical reaction mainly takes place on the cathode side, and the optimal design shows a more uniform distribution of oxygen in that side. Because of the larger contact area of the flow channel and diffusion layer in the optimal design, oxygen can move from the channel to the diffusion layer more easily, and then diffuse uniformly in the diffusion layer. Thus, more reactants can participate in the electrochemical reaction in the catalyst layer. As a result, the PEMFC performance is improved.

5. Conclusion

This study developed a basic design of a three-dimensional PEMFC model and the genetic algorithm was applied to optimize the cross-section shape of the channel. In the optimization process, the width of the bottom and top edges of the channel were considered as variables. The output power and power consumption of flow were the evaluation criteria for the performance of a PEMFC. After the optimization process, a trapezoidal channel whose widths of the bottom and top edges were 1.2874 mm and 0.886 mm, respectively, showed the best performance. At an operating potential of 0.5 V, the power consumption of flow and output power of the optimal design were 3.25% and 8.09% greater than those of the basic design, respectively. In addition, because of the larger contact area of the flow channel and diffusion layer, the optimal design provided more uniform distributions of reactants and current density.

Acknowledgments

This project was supported in part by the National Natural Science Foundation of China No. 51376069 and the National Key Basic Research Program of China (973 Program) No. 2013CB228302.

References

[1] T. Berning, D.M. Lu, N. Djilali, Three-dimensional computational analysis of transport phenomena in a PEM fuel cell, J. Power Sources 106 (1) (2002) 284–294.
[2] N. Ahmadi, S. Rezazadeh, I. Mirzaee, et al., Three-dimensional computational fluid dynamic analysis of the conventional PEM fuel cell and investigation of prominent gas diffusion layers effect, J. Mech. Sci. Technol. 26 (8) (2012) 2247–2257.
[3] D.H. Ahmed, H.J. Sung, Effects of channel geometrical configuration and shoulder width on PEMFC performance at high current density, J. Power Sources 162 (1) (2006) 327–339.
[4] A.P. Manso, F.F. Marzo, M.G. Mujika, et al., Numerical analysis of the influence of the channel cross-section aspect ratio on the performance of a PEM fuel cell with serpentine flow field design, Int. J. Hydrogen Energy 36 (11) (2011) 6795–6808.
[5] Y.G. Yoon, W.Y. Lee, G.G. Park, et al., Effects of channel and rib widths of flow field plates on the performance of a PEMFC, Int. J. Hydrogen Energy 30 (12) (2005) 1363–1366.
[6] M. Bilgili, M. Bosomoiu, G. Tsotridis, Gas flow field with obstacles for PEM fuel cells at different operating conditions, Int. J. Hydrogen Energy 40 (5) (2015) 2303–2311.
[7] S. Shimpalee, J.W. Van Zee, Numerical studies on rib & channel dimension of flow-field on PEMFC performance, Int. J. Hydrogen Energy 32 (7) (2007) 842–856.
[8] H.C. Liu, W.M. Yan, C.Y. Soong, et al., Reactant gas transport and cell performance of proton exchange membrane fuel cells with tapered flow field design, J. Power Sources 158 (1) (2006) 78–87.
[9] F. Tiss, R. Chouikh, A. Guizani, A numerical investigation of reactant transport in a PEM fuel cell with partially blocked gas channels, Energy Convers. Manage. 80 (2014) 32–38.
[10] H.C. Liu, W.M. Yan, C.Y. Soong, et al., Effects of baffle-blocked flow channel on reactant transport and cell performance of a proton exchange membrane fuel cell, J. Power Sources 142 (1) (2005) 125–133.

[11] J.K. Kuo, T.H. Yen, Three-dimensional numerical analysis of PEM fuel cells with straight and wave-like gas flow fields channels, J. Power Sources 177 (1) (2008) 96–103.
[12] M. Hu, A. Gu, M. Wang, et al., Three dimensional, two phase flow mathematical model for PEM fuel cell: Part I. Model development, Energy Convers. Manage. 45 (11) (2004) 1861–1882.
[13] M. Hu, X. Zhu, M. Wang, et al., Three dimensional, two phase flow mathematical model for PEM fuel cell: Part II. Analysis and discussion of the internal transport mechanisms, Energy Convers. Manage. 45 (11) (2004) 1883–1916.
[14] X.D. Wang, W.M. Yan, Y.Y. Duan, et al., Numerical study on channel size effect for proton exchange membrane fuel cell with serpentine flow field, Energy Convers. Manage. 51 (5) (2010) 959–968.
[15] X.D. Wang, Y.Y. Duan, W.M. Yan, Novel serpentine-baffle flow field design for proton exchange membrane fuel cells, J. Power Sources 173 (1) (2007) 210–221.
[16] R. Roshandel, F. Arbabi, G.K. Moghaddam, Simulation of an innovative flow-field design based on a bio inspired pattern for PEM fuel cells, Renewable Energy 41 (2012) 86–95.
[17] H.C. Chiu, J.H. Jang, W.M. Yan, et al., A three-dimensional modeling of transport phenomena of proton exchange membrane fuel cells with various flow fields, Appl. Energy 96 (2012) 359–370.
[18] T. Henriques, B. César, P.J.C. Branco, Increasing the efficiency of a portable PEM fuel cell by altering the cathode channel geometry: a numerical and experimental study, Appl. Energy 87 (4) (2010) 1400–1409.
[19] S.W. Perng, H.W. Wu, T.C. Jue, et al., Numerical predictions of a PEM fuel cell performance enhancement by a rectangular cylinder installed transversely in the flow channel, Appl. Energy 86 (9) (2009) 1541–1554.
[20] S. Lee, H. Jeong, B. Ahn, et al., Parametric study of the channel design at the bipolar plate in PEMFC performances, Int. J. Hydrogen Energy 33 (20) (2008) 5691–5696.
[21] S.W. Perng, H.W. Wu, Non-isothermal transport phenomenon and cell performance of a cathodic PEM fuel cell with a baffle plate in a tapered channel, Appl. Energy 88 (1) (2011) 52–67.
[22] X.D. Wang, Y.X. Huang, C.H. Cheng, et al., Flow field optimization for proton exchange membrane fuel cells with varying channel heights and widths, Electrochim. Acta 54 (23) (2009) 5522–5530.
[23] W.J. Yang, H.Y. Wang, Y.B. Kim, Channel geometry optimization using a 2D fuel cell model and its verification for a polymer electrolyte membrane fuel cell, Int. J. Hydrogen Energy 39 (17) (2014) 9430–9439.
[24] B.R. Sivertsen, N. Djilali, CFD-based modelling of proton exchange membrane fuel cells, J. Power Sources 141 (1) (2005) 65–78.
[25] L. Wang, A. Husar, T. Zhou, et al., A parametric study of PEM fuel cell performances, Int. J. Hydrogen Energy 28 (11) (2003) 1263–1272.
[26] T. Berning, N. Djilali, Three-dimensional computational analysis of transport phenomena in a PEM fuel cell—a parametric study, J. Power Sources 124 (2) (2003) 440–452.
[27] B. Rismanchi, M.H. Akbari, Performance prediction of proton exchange membrane fuel cells using a three-dimensional model, Int. J. Hydrogen Energy 33 (1) (2008) 439–448.
[28] M.S. Chiang, H.S. Chu, Numerical investigation of transport component design effect on a proton exchange membrane fuel cell, J. Power Sources 160 (1) (2006) 340–352.
[29] H. Meng, A two-phase non-isothermal mixed-domain PEM fuel cell model and its application to two-dimensional simulations, J. Power Sources 168 (1) (2007) 218–228.
[30] X. Liu, W. Tao, Z. Li, et al., Three-dimensional transport model of PEM fuel cell with straight flow channels, J. Power Sources 158 (1) (2006) 25–35.
[31] Y. Ge, Z. Liu, W. Liu, et al., Active optimization design theory and method for heat transfer unit and its application on shape design of cylinder in convective heat transfer, Int. J. Heat Mass Transfer 90 (2015) 702–709.
[32] Y. Ge, Z. Liu, W. Liu, Multi-objective genetic optimization of the heat transfer for tube inserted with porous media, Int. J. Heat Mass Transfer 101 (2016) 981–987.